Available online at http://ijcpe.uobaghdad.edu.iq and www.iasj.net
Iraqi Journal of Chemical and Petroleum Engineering
Vol. 24 No. 4 (December 2023) 31 – 37
EISSN: 2618-0707, PISSN: 1997-4884

CFD Simulation of Methanol Dehydration Step through an Adiabatic Fixed-bed Reactor of DME Synthesis

Roozbeh Mofidian [a, *], Mojtaba Jahanshahi [b], Seyed Sharafoddin Hosseini [c], Mehdi Miansari [c]

a Department of Chemical Engineering, Technical and Vocational University (TVU), Tehran, Iran
b Nanotechnology Research Institute (NRI), Excellence Centre of Nanotechnology in Water, School of Mechanical Engineering, Babol Noshirvani University of Technology, Babol, Iran
c Depatment of Mechanical Engineering, Technical and Vocational University (TVU), Tehran, Iran

Abstract

Today, dimethyl ether (DME) is changing to ordinarily worn as a superb aerosol propellant and refrigerant for its eco-friendly characteristics. Lately, with the development of novel chemical energy in the coal industries, it has become a fascinating field of research as an alternative green fuel for diesel machines due to the high cetane number. The DME synthesis processes include catalytic dehydrating methanol in an adiabatic fixed-bed reactor. In this study, to investigate the chemical conditions of the methanol dehydration reaction, CFD simulations of the adiabatic reactor have been assessed. The advantage of the work is a sensitivity analysis was run to find the effect of pressure, kinetics, and velocity on the reactor performance. The results showed that using a γ-Al_2O_3 catalyst with selective mechanical properties and unique surface properties is a convenient choice for DME synthesis. The CFD simulation results also show that the laboratory data such as pressure, energy, and velocity in the adiabatic reactor meet the reaction requirements well, and deliberated a major vision of what happened in the reactor. Also, the graphs of the temperature profile with changes in physical properties pomp that methanol dehydration reaction strongly depends on environmental factors and gives different results under the influence of other conditions.

Keywords: CFD, DME, Energy, Methanol Dehydration, Simulation.

Received on 05/10/2023, Received in Revised Form on 21/11/2023, Accepted on 24/11/2023, Published on 30/12/2023

https://doi.org/10.31699/IJCPE.2023.4.3

1- Introduction

The most logical way to reduce greenhouse gases (the leading cause of air pollution) is to replace clean and renewable power plants with thermal power plants. One of the problems we constantly face is global warming and air pollution [1]. This heating, as well as pollution, is caused by the overproduction of greenhouse gases. Forty billion tons of these gases enter the air annually. Global studies on greenhouse gases show that thermal power plants have the highest share of greenhouse gas emissions (about 22%) [2]. Iran is the eighth largest greenhouse gas producer, producing 800 million tons of greenhouse gases annually [3]. Greenhouse gases are the primary source of air and environmental pollution, which causes the most significant ecological problems. Increasing renewable energy, especially wind and solar, is crucial to achieving this ambitious goal. Large-scale and long-term energy storage will also play a key role [4].

Iran has one of the world's most enormous gas resources due to its vibrant natural gas reserves, especially in the South Pars region in the Persian Gulf. Proximity to world markets, especially in South Asia and Europe, has made Iran one of the safest and most economical countries with natural gas, which has an undeniable role in the Middle East. Methanol production technology from synthetic gas is a well-known process [5]. However, in synthesizing methanol, due to the reversible nature of this material's production reaction, achieving the maximum conversion rate of the synthesized gas in one pass through the reactor is limited [6]. Simultaneous conversion of methanol to other chemicals, such as olefins and DME, can be an excellent solution to reduce the methanol synthesis reaction's equilibrium limit [7]. DME is one of the essential products of chemical conversion of natural gas, which seems economically necessary [8].

Due to the astonishing increase in population and the urgent need to improve living standards, the amount of energy consumption in the world has been accompanied by a more significant acceleration [9]. Today, most energy sources in the world are supplied by fossil fuels, leading to worsening environmental conditions and increasing additional costs in the long run. Therefore, using green instead of fossil fuels has become a necessity and ecological demand. DME, which is known as a clean

*Corresponding Author: Name: Roozbeh Mofidian, Email: roozbeh.mofidian@yahoo.com

and environmentally friendly fuel, is attracting increasing attention [10].

DME is a volatile substance that liquefies at a pressure of about 1 MPa, and a temperature of 25 ˚C. Since the flame produced from it is blue and has similar properties to propane and butane, it is used as liquefied petroleum gas (LPG) for domestic use. So, according to the features mentioned, in the future, DME will be a large part of the alternative to conventional fuels today [11]. CN of DME is optimally high, so it is used as a substitute for diesel, and its combustion exhaust gas is much cleaner than diesel. DME produced raw materials, including natural gas, crude oil, refined oil, coal, and waste products [12]. Natural gas is the best choice among the above reactors due to its cheapness and availability. Production of DME from natural gas allows the investor to mass produce independently of fluctuations in world oil prices [13]. Due to its chemical nature, LPG is an octane fuel, and DME is a cetane fuel. The same indicator causes the replacement of diesel fuel during combustion. Because DME produces the least amount of NOx and CO, it acts as a clean fuel when burned in engines optimized for DME use [14]. Table 1 shows DME and other related fuels' physical properties and combustion characteristics.

Table 1. Physical Properties of DME and other Fuels

Properties	Boiling point (K)	Liquid density (g/cm3)	Vap. Pressure (atm)	Ignition temperature (K)	Explosion limit	Cetane number	Net calorific value (10^6J/kg)
DME	247.9	0.67	66.1	623	3.4-1.7	55-60	28.90
Propane	231	0.49	9.3	777	2.1-9.4	5	46.46
Methane	111.5	-	-	905	5-15	0	50.23
Methanol	337.6	0.79	-	743	5.5-36	5	21.1
Diesel	180-370	0.84	-	-	0.6-6.5	40-55	41.86

DME production capacity has been growing and is approximately 9 million tons annually [15]. Due to plans to build several plants, it is predictable that DME production will increase significantly in the next decade, especially in Asia [16]. DME requires 75 psi of pressure to be liquid, which is why DME management requirements are very similar to propane. Both must be stored in pressurized storage tanks at ambient temperature, and conventional DME production produces carbon monoxide from the synthesized gas [17]. The latest recognition of DME synthesis from NO_x as a potential resource to moderate global CO_2 production has further added to the growing interest in DME synthesis [18]. The above features make DME a clean fuel for the next century. As mentioned earlier, using synthetic gas as raw material, DME can be produced in a one-step process. All these steps are exothermic reactions, so the final response is an entirely exothermic process. Table 2 shows reactions concerning DME synthesis and their reaction heat. The direct synthesis of DME topics essentially focuses on the discrimination of bifunctional catalysts, the development of different kinetic models, and the relevant reactor design of CFD simulation in a fixed-bed reactor.

Table 2. Reactions of DME Synthesis

No.	Reaction	Reaction name	Reaction heat
1	$3CO + 3H_2 \leftrightarrow CH_3OCH_3 + CO_2$	Overall 1	-256.615
2	$2CO + 4H_2 \leftrightarrow CH_3OCH_3 + H_2O$	Overall 2	-205
3	$2CO + 4H_2 \leftrightarrow 2CH_3OH$	Methanol synthesis	- 181.6
4	$2CH_3OH \leftrightarrow CH_3OCH_3 + H_2O$	Methanol dehydration	-21.255
5	$CO + H_2O \leftrightarrow CO_2 + H_2$	Water-gas shift	-40.9

In Table 2, all reactions are reversible and exothermic. According to the equations mentioned above, the direct method has been used, and the methanol synthesis reaction from syngas takes place in the reactor. The general reactions (1) and (2) are initiated by a suitable catalyst (Cu / ZnO / Al_2O_3), and an acidic catalyst catalyzes reaction (3). Methanol dehydration reaction occurs in the gas phase and is almost exothermic. The heat of the reaction is much lower than in a one-step process [19]. Of course, this method is fully proven in large-scale plants. For this reason, commercial production of DME is carried out in a reactor with a fixed adiabatic substrate in the temperature range of 200 ° C to 400 °C and at pressures up to 2 MPa on γ-Al_2O_3 catalysts and synthetic molecular sieve materials. Many authors focused on the kinetic of reaction (4) and as below:

$$r_{Methanol} = k{f_{Methanol}}^2\left(1 - \frac{f_{DME}f_{water}}{K_{eq}{f_{Methanol}}^2}\right) \quad (1)$$

Where f is fugacity and K_{eq} is:

$$k = 1457exp\left(-\frac{78072}{RT}\right) \quad (2)$$

$$lnK_{eq} = -26.64 + 3.7\ lnT + \frac{4019}{T} - 2.78 \times 10^{-3}T + 3.8 \times 10^{-7}T^2 - 6.56 \times 10^4 T^3 \quad (3)$$

In the second natural reaction, syngas is used to feed the process. In this process, the syngas is first converted to methanol, then the dewatering methanol to DME [20]. Another method for directly synthesizing DME is using a two-phase fluidized bed reactor, which has been experimentally proven more effective than CO slurry reactors [21]. The results showed that the conversion of methanol strongly depends on the reactor's operating

temperature. This work used acidic γ-Al_2O_3 as a catalyst for dewatering methanol to DME [22]. We also reached the optimal weight hourly space velocity (WHSV), which gives us the maximum methanol conversion at three methanol gas inlet temperatures. One of the benefits of this work is the use of dynamic simulation to determine physical conditions such as temperature and pressure. Understanding the mechanical and thermal properties that take place in the adiabatic reactor is only possible by applying accurate boundary conditions in dynamic calculations.

This study analyzed CFD simulation of the methanol dehydration step through an adiabatic fixed-bed DME synthesis reactor. The goal is to learn the reactor's dynamic characteristics, such as pressure, kinetic energy, and velocity magnitude. This knowledge is essential for enhancing the synthesis technology of DME, understanding the formation or process, and modeling the various performance measures required for process control and optimization. For this purpose, CFD analysis is viable because direct measurement of pressure, kinetic energy, and particle velocities are complicated. This paper establishes CFD models for dynamic properties using the Fluent 18 flow solver. The operating conditions for the methanol dehydration process are shown below in Table 3.

Table 3. Operating Conditions for the Methanol Dehydration Process

Parameters	Values
Catalyst particle	
Density	2010
Particle diameter	$0.3175*10^{-2}$
Specific surface area	673
The ratio of void fraction to tortuosity of the catalyst particle	0.066
Fixed bed reactor	
Length of reactor	8.06
Bed void fraction	0.5
The density of the catalyst bed	1005
Wall thermal conductivity	48
Diameter of reactor	4
Feed composition	
CH_3OH	0.936
DME	0.055
H_2O	0.009
Mass flow rate	50.81
Inlet pressure	18.18
Inlet temperature	533

2- CFD Methods

The primary governing equations used to form the CFD model, and the simulation study's boundary conditions are given below.

$$\frac{\partial \rho}{\partial t} + \frac{\partial (\rho \vartheta_i)}{\partial y_i} = m_m \quad (4)$$

In this equation, m_m Contains the mass added through phase changes or user-defined sources. Generally, and in the simulations described here, the source term was equal to zero. Navier-Stokes equations were utilized for the description of the momentum changes. The equation for conservation of momentum is defined by:

$$\frac{\partial (\rho \vartheta_i)}{\partial t} + \frac{\partial (\rho \vartheta_i \vartheta_j)}{\partial y_j} + \frac{\partial \rho}{\partial y_i} + \frac{\partial \emptyset_{ij}}{\partial y_i} = \rho g_i \quad (5)$$

Where ρg is the gravitational body force, and τ is the stress tensor. The below equation defines the stress tensor:

$$\emptyset_{ij} = \left(\frac{2}{3}\mu - \epsilon\right)\delta_{ij}\frac{\partial \vartheta_k}{\partial y_k} - \mu\left[\frac{\partial \vartheta_i}{\partial y_j} + \frac{\partial \vartheta_j}{\partial y_i}\right] \quad (6)$$

Where δ_{ij} is the Kronecker delta function as below:

$$\frac{\partial (\rho Y_i)}{\partial t} + \frac{\partial (\rho Y_i \vartheta_j)}{\partial y_j} + \frac{\partial (j_{i,j})}{\partial y_j} = Net \quad (7)$$

$$j_{i,j} = -(\rho \frac{Y_i}{X_i} {D_i}^e \frac{\partial X_i}{\partial y_j}) + \frac{{D_i}^t}{T}\frac{\partial T}{\partial y_j}$$

$$X_i = \frac{1}{\sum \frac{Y_j}{M_j}}\frac{Y_i}{M_i}$$

The energy equation was solved in the form of the transport equation for a static temperature. The energy equation is obtained from the enthalpy balance taking the temperature as a dependent variable. The enthalpy equation balance is defined as:

$$\frac{\partial (\rho h)}{\partial t} + \frac{\partial (\rho h \vartheta_j)}{\partial y_j} + \frac{\partial j_{q,j}}{\partial y_j} = \frac{\partial p}{\partial t} + \vartheta_j \frac{\partial p}{\partial y_j} - \emptyset_{jk}\frac{\partial \vartheta_j}{\partial y_k} + m_h \quad (8)$$

$$j_{q,j} = -\omega \frac{\partial T}{\partial y_j} + \sum h_i j_{i,j}$$

$$h = \sum Y_i h_i(T)$$

$$P = \frac{\rho RT}{\sum X_i M_i}$$

3- Results

3.1. Validation

The simulation is validated from the literature by Samimi et al. [23] For conditions listed in Table 3. Because the developed DME synthesis process is not industrial, the validity of each modeling component is confirmed individually. In the meantime, the developed model is updated based on the dimensions and feed characteristics of industrial reactors, and the simulated results are matched with the output of factory data. The developed models seem accurate and can be used for the flue gas conversion process to DME. The simulation results show a good agreement with the published experimental data.

3.2. CFD Simulation

CFD simulations have been performed to investigate the reaction conditions of DME synthesis in an adiabatic fixed-bed reactor. The mixing rate of materials and their physical properties are given in Table 4.

The assumed catalyst thermal properties are presented in the table, which corresponds to the alumina. The different steps of DME synthesis are exposed in Fig. 1. The middle reactor has a diameter of 2 cm, a height of 90 cm, an inlet hole of 2 cm, and an outlet of 1 cm. The inlet feed enters the reactor with a flow rate of 1 cm/s and has 25 °C and 1 bar for temperature and pressure,

respectively. The type of flow regime is considered laminar flow according to CFD calculations.

Table 4. Materials and the Physical Properties of Synthesis

Parameters Materials	Methanol	DME	Water	Alumina
Weight percentage (%)	48	25	25	2
Density (g/cm^3)	792	2.11	1	2.1
Viscocity (Kg/m.s)	0.545	1	1	-
Specific heat capacity (J/g.K)	2.4	65.6	4.2	1
Thermal conductivity (W/m.K)	0.1	1	0.6	1

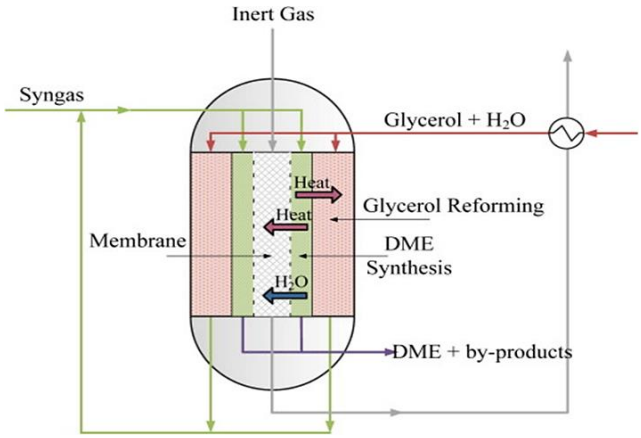

Fig. 1. Schematic Diagram of DME Synthesis

In this paper, 0.6 particle sphericity was used to calculate the surface roughness. Experimental experiments were considered in the pressure range of 2-4 MPa and H_2/CO ratio of 0.6 to 1.8. A constant gas space velocity of 2800 ml/g cat/h (STP) was used throughout the test. A transient simulation of the reactor tested is collected here. In all CFD simulation experiments, the boundary condition of constant wall temperature was observed (T=298 K). All experiments were repeated three times, and the steady state diagram was drawn based on the respective inputs and outputs to be stable and reliable in the simulation. The graph of the output molar fraction in terms of the flow rate-time ratio, as expected from the simulation behavior, is shown in Fig. 2. Often, the exhaust gas composition and flow rate approach relatively constant values at a retention time. Meantime values are used to evaluate the steady-state performance of the reactor to eliminate the effect of small oscillations in the output currents.

The axial indices of the volume fraction of solids and the molar fractions of CO, H_2, and DME for the H_2/CO input ratio of 1.0 and the reactor pressure of 3 MPa are shown in Fig. 3. The length of the bed was increased to a height of about 90 cm to maintain the physical condition of the experiment, gradually the volume fraction of solids increases along the reactor because the volume of the gas (molar) of the stream decreases due to adverse reactions. CO and H_2 decreased as the responses consumed them, and methanol and DME concentrations increased along the reactor length. Similar behaviors were observed for other variables, such as reactor pressure and H_2 /CO ratio. Due to the boundary conditions of fixed wall temperature and the small diameter of the reactor, the maximum temperature increase of less than 5 K is reported. Also, the molar fraction of water (not shown in the figure) remained less than 0.01 throughout the reactor because most of the water produced by methanol synthesis and dehydration reactions was consumed during the reaction. The results of this part of the research are consistent with the published data from the work of Moradi et al. By investigating and simulating the fixed-bed reactor, they showed, that the effect of the exothermic nature of reactions appeared earlier in an isothermal fixed-bed reactor than in an adiabatic fixed-bed reactor.

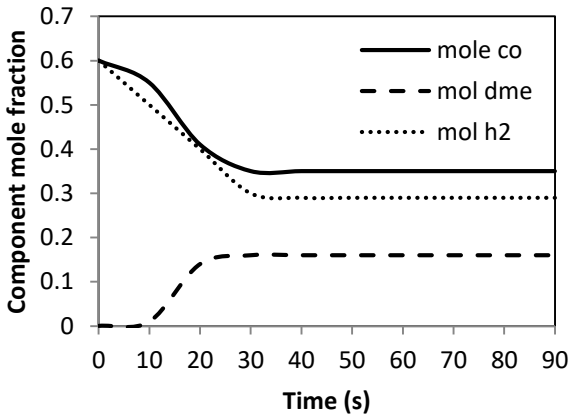

Fig. 2. Outlet Stream Composition versus Reaction Time

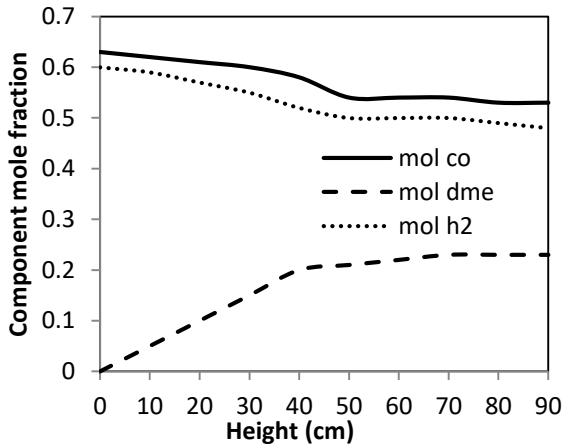

Fig. 3. Profile Plots of Component Compositions at t=60 s

3.3. Mesh Study

The geometry of the reactor is done considering the boundary conditions and using Gambit software. Moreover, due to the cylindrical geometry utilized, in some places, the elements were hexagonal, pyramidal, and quadrilateral, hence refined meshing was necessary near the wall. The details of its mesh structure are shown in Fig. 4. The most crucial step in CFD simulation is to evaluate network independence. As you can see, the reaction is simulated in many networks with different cell sizes. After that, the change of various parameters in different meshes in cell size of about 0.034 cm. So, for

this work, we used a grid of this size. The finite volume method was used with ANSYS FLUENT software to solve the equations. Mass-flow-inlet and outflow boundary conditions were used for the reactor inlet and outlet, respectively. The assumptions implemented in the present work are as follows:

-Catalyst was not considered.

-Steady-state conditions and ideal gas law were conducted.

-A pressure-based module was used to solve the equation.

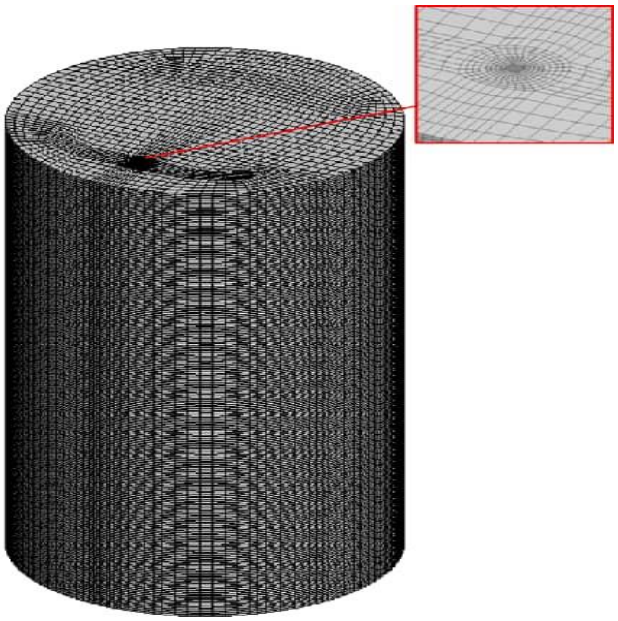

Fig. 4. Mesh Formatting of the Reactor

Fig. 5 shows a CFD simulation of the intermediate reactor in the DME synthesis reaction. Pressure, energy, and velocity contours are good indicators of the effectiveness of chemicals inside the reactor. The pressure contour indicates that the pressure gradually increases during the reactor from bottom to top. The energy contour indicates the maximum energy distribution in the middle of the reactor. The velocity contour also shows that the velocity in the reactor's central axis is higher than the direction of the reactor and is minimal near the walls. The results of this research are in good agreement with the results of Golshadi et al., and while they investigated the temperature contour along the reactor, our work shows more detailed investigations.

3.4. Heat Transfer

Fig. 6 shows the effect of the inlet temperature change on the temperature profile inside the reactor. The results indicate that as the inlet temperature increases, the temperature profile and reactor temperature rise and reach the maximum point. This perceptible temperature change increases intermittently with the increase of the inlet temperature to the reactor. Fig. 7 shows the effect of flow velocity entering the reactor regarding the temperature profile. As can be seen, with increasing input speed, the temperature profile increases, and at higher rates, this increase is more considerable. For example, the temperature difference at an inlet velocity of 1 cm/s is about 19 °C along a length of 1 cm and about 23 °C at a velocity of 1.5 cm/s. Fig. 8 shows the effect of inlet pressure on the temperature profile. With increasing inlet pressure, the temperature profile increases and gradually decreases after reaching the maximum point and finally gets a fixed position along the reactor.

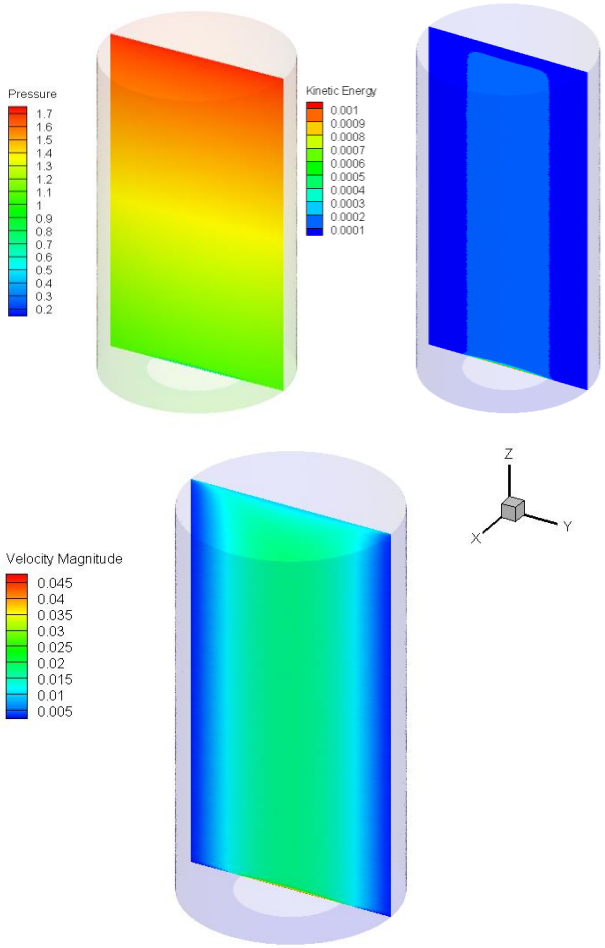

Fig. 5. CFD Simulation of the Middle Reactor Pressure, Kinetic Energy, and Velocity Magnitude, Respectively, from Left to Right

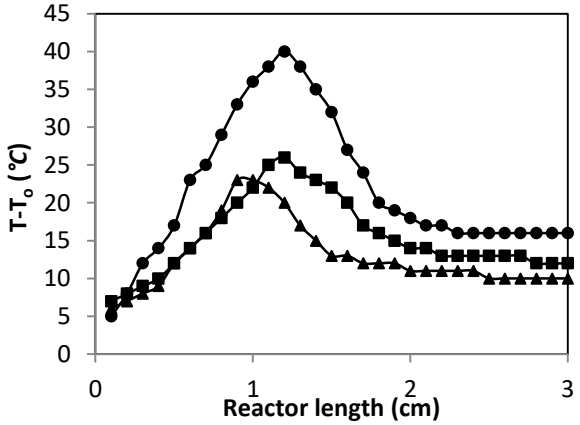

Fig. 6. Effect of Change in Inlet Temperature on Reactor Temperature Profile; (●) T=30 °C, (■) T=25 °C, (▲) T=20 °C

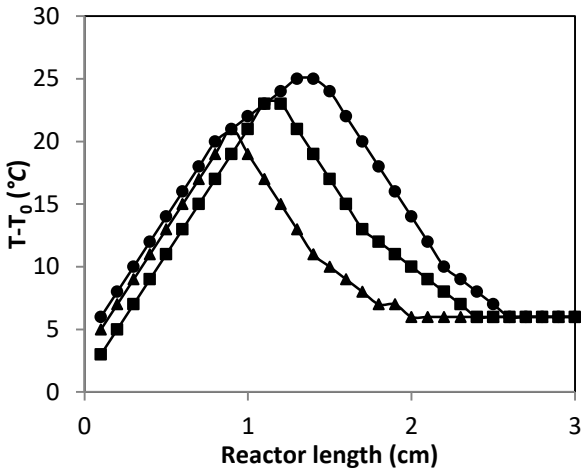

Fig. 7. Effect of Change in Terminal Velocity on Reactor Temperature Profile; (●) u=1.5 cm/s, (■) u=1 cm/s, (▲) u=0.5 cm/s

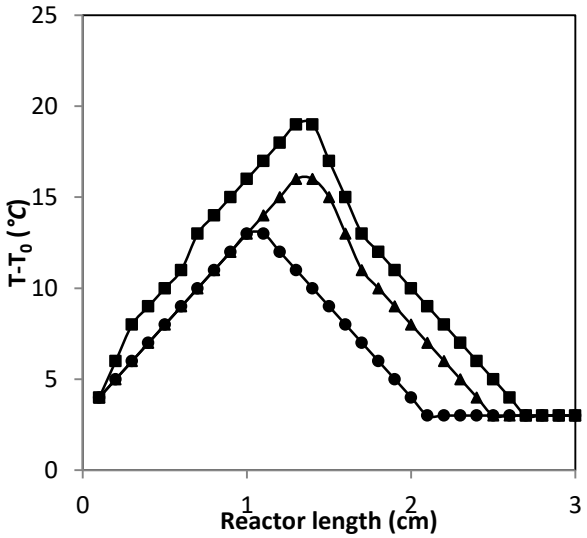

Fig. 8. Effect of Change in Pressure on Reactor Temperature Profile; (●) P=1 bar, (■) P=1.5 bar, (▲) P=2 bar

4- Conclusion

In this study, the synthesis of DME in a fixed-bed reactor was investigated. The simulation of this reactor was done by ANSYS Fluent Software. The reactor has a diameter of 2 cm, a height of 90 cm, an inlet hole of 2 cm, and a laminar flow rate of 1 cm/s and has 25 °C and 1 bar for temperature and pressure, respectively. The methanol dehydration step inside the adiabatic reactor was assessed by the CFD method. For the geometry section the change of various parameters in different meshes in cell size of about 0.034 cm. The catalyst used in this process was synthesized alumina with a porous size of 4.54 µm, whose physical properties and surface morphology were investigated. The temperature profile in different temperatures, pressure, and speed velocities were analyzed to investigate the heat transfer properties of the reaction inside the reactor. The results showed that the adiabatic fixed-bed reactor's temperature profile increases with increasing temperature, pressure, and velocity. The results of heat transfer calculations showed that most of the temperature changes occur at the beginning of 25% of the length of the reactor. Outlet mole fractions component versus time diagram shows that DME synthesis directly depends on time and reactor length. This study affirms that the detailed CFD model can be used as a tool to determine conditions for successful synthesis operations with different conditions. The techniques of this study are applicable for implementation in a real factory or an industrial plant, and there is reliable information for the results of this research. Ultimately, the CFD modeling results generated in the present work showed reasonable agreement with previously obtained data available in the literature. It is suggested that future studies be conducted to deal with the kinetic inhibition of DME formation related to the presence of water. Moreover, the promising approach of realizing a DME membrane reactor would not be out of mind. Especially in this context, CFD modeling is a relevant tool that offers the possibility of changing geometries without the detailed and time-consuming construction of different reactor geometries.

Nomenclature

DME	Dimethyl Ether
CFD	Computational Fluid Dynamic
LPG	Liquefied Petroleum Gas
CN	Cetane Number
WHSV	Weight Hourly Space Velocity
STP	Standard Temperature and Pressure

References

[1] Z.I. Rony, M. Mofijur, M.M. Hasan, M.G. Rasul, M.I. Jahirul, S.F. Ahmed, M.A. Kalam, I.A. Badruddin, T.M.Y. Khan, P.-L. Show. Alternative fuels to reduce greenhouse gas emissions from marine transport and promote UN sustainable development goals. *Fuel*, (338), 2023, 127220. https://doi.org/10.1016/j.fuel.2022.127220

[2] R. Mofidian, A. Barati, M. Jahanshahi, M. H. Shahavi. Optimization on thermal treatment synthesis of lactoferrin nanoparticles via Taguchi design method. *SN Applied Sciences*, (1), 2019, 1-9. https://doi.org/10.1007/s42452-019-1353-z

[3] F. Chien, C.C. Hsu, I. Ozturk, A. Sharif, M. Sadiq. The role of renewable energy and urbanization towards greenhouse gas emission in top Asian countries: Evidence from advance panel estimations. *Renewable Energy*, (186), 2022, 207-216. https://doi.org/10.1016/j.renene.2021.12.118

[4] R. Mofidian, Q. Xiong, A.M. Ranjbar, M.A. Sabbaghi, A., Farhadi, S.M. Alizadeh. Adsorption of lactoferrin and bovine serum albumin nanoparticles on pellicular two-layer agarose-nickel at reactive blue 4 in affinity chromatography. *Journal of Environmental Chemical Engineering*, 2 (9), 2021, 105084. https://doi.org/10.1016/j.jece.2021.105084

[5] N. Maroufi, N. Hajilary. The impacts of economic growth, foreign direct investments, and gas consumption on the environmental Kuznets curve hypothesis CO2 emission in Iran. *Environmental Science and Pollution Research*, 2022, 1-14. https://doi.org/10.1007/s11356-022-20794-x

[6] R. Mofidian, A. Barati, M. Jahanshahi, M.H.Shahavi. Generation process and performance evaluation of engineered microsphere agarose adsorbent for application in fluidized-bed systems. *International Journal of Engineering*, 8 (33), 2020, 1450-1458. https://doi.org/10.5829/IJE.2020.33.08B.02

[7] R. Babaei, A. Farrokhabadi. Predicting the debonding formation and induced matrix cracking evolution in open-hole composite laminates using a semi-consequence micro-macro model. *Composite Structures*, (210), 2019, 274-293. https://doi.org/10.1016/j.compstruct.2018.11.017

[8] R. Mofidian, A. Barati, M. Jahanshahi, M.H. Shahavi. Fabrication of novel agarose–nickel bilayer composite for purification of protein nanoparticles in expanded bed adsorption column. *Chemical Engineering Research and Design*, 8 (159), 2020, 291-299. https://doi.org/10.1016/j.cherd.2020.03.024

[9] N. S. Ahmedzeki, B. J. Ibrahem. Reduction of sulfur compounds from petroleum fraction using oxidation-adsorption technique. *Iraqi Journal of Chemical and Petroleum Engineering*, 1 (16), 2015, 35-48. https://doi.org/10.31699/IJCPE.2015.1.4

[10] M. Zastempowski. Analysis and modeling of innovation factors to replace fossil fuels with renewable energy sources-Evidence from European Union enterprises. *Renewable and Sustainable Energy Reviews*, (178), 2023, 113262. https://doi.org/10.1016/j.rser.2023.113262

[11] G.T. Hashem, Al-Dawody, M.F. Use of LPG in SI engine-a review study. *Al-Qadisiyah J Eng Sci*, 2 (14), 2021, 54-61. https://doi.org/10.30772/qjes.v14i1.751

[12] R. Babaei, A. Farrokhabadi. Prediction of debonding growth in two-dimensional RVEs using an extended interface element based on continuum damage mechanics concept. *Composite Structures*, (238), 2020, 111981. https://doi.org/10.1016/j.compstruct.2020.111981

[13] H.H. Koybasi, A.K. Avci. Numerical Analysis of CO2-to-DME Conversion in a Membrane Microchannel Reactor. *Industrial & Engineering Chemistry Research*. 2022. https://doi.org/10.1021/acs.iecr.2c01764

[14] S.Munahar, B.C. Purnomo, M. Setiyo, A. Triwiyatno, J.D. Setiawan. Design and application of air to fuel ratio controller for LPG fueled vehicles at typical down-way. *SN Applied Sciences*, 1 (2), 2020, 1-7. https://doi.org/10.1007/s42452-019-1839-8

[15] S.N. Sajedi, M.E. Masoumi, K. Movagharnejad. Exergetic improvement and environmental impact assessment of crude oil distillation unit of Shazand-Arak oil refinery. *International Journal of Exergy*, 4 (16), 2015, 464-480. https://doi.org/10.1504/IJEX.2015.069116

[16] A. Rezvani, Y. Li, S. Neumann, O. Anwar, D. Rafaja, S. Reichenberger, D. Segets. Stability of Binary Colloidal Mixtures of Au Noble Metal and ZnS Semiconductor Nanoparticles. *Colloids and Surfaces A: Physicochemical and Engineering Aspects*. 2024. https://doi.org/10.1016/j.colsurfa.2023.132832

[17] M. Masoumpour-Samakoush, M. Miansari, S.S.M. Ajarostaghi, M. Arıcı. Impact of innovative fin combination of triangular and rectangular fins on melting process of phase change material in a cavity. *Journal of Energy Storage*, (45), 2022, 103545. https://doi.org/10.1016/j.est.2021.103545

[18] A.S. Amarasekara, L.H. Nguyen, H. Du, R.R. Kommalapati. Kinetics and mechanism of the solid-acid catalyzed one-pot conversion of d-fructose to 5, 5′-[oxybis (methylene)] bis [2-furaldehyde] in dimethyl sulfoxide. *SN Applied Sciences*, 9 (1), 2019, 1-7. https://doi.org/10.1007/s42452-019-0994-2

[19] S. Hosseinzadeh, M. Jahanshahi, A. Rahbari, P. Molaghan, Q. Xiong, S. Vahedi, S. Sadeghi. Oscillating transient flame propagation of biochar dust cloud considering thermal losses and particles porosity. *Combustion and Flame*, (234), 2021, 111662. https://doi.org/10.1016/j.combustflame.2021.111662

[20] H. Khaksar and M. Jahanshahi, "Control of indentation depth in nanomanipulation process to avoid damage of microparticles," *2019 7th International Conference on Robotics and Mechatronics (ICRoM)*, Tehran, Iran, 2019, pp. 593-598, https://doi.org/10.1109/ICRoM48714.2019.9071796

[21] M. Jahanshahi, R. Mofidian, S.S. Hosseini, M. Miansari. Investigation of mechanical properties of granular γ-alumina using experimental nano indentation and nano scratch tests. *SN Applied Sciences*, 6 (5), 2023, 164. https://doi.org/10.1007/s42452-023-05388-7

[22] R. Mofidian, M.H. Shahavi, A. Barati, M. Jahanshahi, Engineering mechanisms for protein nanoparticles adsorption, pp. 866-871, 2019.

[23] F. Samimi, M. Bayat, M.R. Rahimpour, P. Keshavarz. Mathematical modeling and optimization of DME synthesis in two spherical reactors connected in series. *Journal of Natural Gas Science and Engineering*, (17), 2014, 33-41. https://doi.org/10.1016/j.jngse.2013.12.006